Numerical investigation of effects of "baffles - deceleration strip" hybrid system on rock avalanches

BI Yu-zhang[1,2]* (iD) https://orcid.org/0000-0003-2631-6620 ; ✉ e-mail: biyuzhang@seu.edu.cn

HE Si-ming[3, 4, 5, 6] (iD) https://orcid.org/0000-0002-9074-9298; e-mail: hsm@imde.ac.cn

DU Yan-jun[1, 2] (iD) https://orcid.org/0000-0001-9533-8976; e-mail: duyanjun@seu.edu.cn

SHAN Jie[1, 2] (iD) https://orcid.org/0000-0003-4775-6158; e-mail: JieShan_TJ@163.com

YAN Shuai-xing[4, 5] (iD) https://orcid.org/0000-0002-4456-5834; e-mail: yansx1991@yeah.net

WANG Dong-po[7] (iD) https://orcid.org/0000-0002-6172-4753; e-mail: wangdongpo2014@cdut.edu.cn

SUN Xin-po[8]* (iD) https://orcid.org/0000-0001-8973-9853; ✉ e-mail: xinpo2008@sina.com.cn

Corresponding Author

1 Institute of Geotechnical Engineering of Southeast University, Nanjing 210096, China

2 School of Transportation Southeast University, Nanjing 210096, China

3 Key Laboratory of Mountain Hazards and Surface Process, Chinese Academy of Sciences, Chengdu 610041, China

4 Institute of Mountain Hazards and Environment, Chinese Academy of Sciences, Chengdu 610041, China

5 Chinese Academy of Sciences Center for Excellence in Tibet Plateau Earth Sciences, Beijing 100101, China

6 University of Chinese Academy of Sciences, Beijing 100049, China

7 State Key Laboratory of Geohazard Prevention and Geoenvironment Protection, Chengdu University of Technology, Chengdu 610059, China

8 College of civil engineering, Sichuan University of Science and Engineering, Zigong 643000, China

Abstract: Arrays of baffles are usually installed in front of protection site to attenuate the flow energy of rock avalanches in mountainous areas. Optimization design is crucial for efficiency promotion in hazard energy dissipation engineering. In this study, a deceleration strip was added in the baffles protection system to optimize the traditional baffles system. The effects of the "baffles - deceleration strip" hybrid protection system was discussed in detail with the nails number and nails angle. This study presents details of numerical experiments using the discrete element method (DEM). The effect of the optimization of hybrid protection system (nail angle and nail number) were investigated specifically, especially the impact force that avalanches exerted on structures. The results show that the maximum impact forces and kinetic energy of the rock avalanches decreases with the increase of the number and angle of the nail. Moreover, the distance between the toe and the bearing structure (L_m) is also a key factor. The shorter the distance L_m (30m) is, the higher the maximum impact force are. The longer the distance L_m (70m) is, the lower the maximum impact force are. Under the same size of the nails, increasing the numbers can enhance the dissipation ability of the hybrid protection system. Meanwhile, increasing its

angle can also enhance the dissipation ability. There are three key ways for nails attenuate rock avalanches: (i) block the fine particles directly; (ii) form the particles bridge between nails and baffles; (iii) dissipate the coarse particles energy directly. The effect of segregation in rock avalanches is crucial for the energy dissipation mechanism, which is a key factor to optimize the traditional baffle system.

Key words: Rock avalanches; Baffles; Hybrid system; Energy dissipation; Impact force

Introduction

Rock avalanche is a kind of collapse hazards which means extremely rapid, massive, flow-like motion of fragmented rock from a large rock slide or rockfalls (Hungr et al. 2014), of which volume ranges from $0.4{\times}10^6$ to $1{\times}10^9$ m^3 . Rock avalanche has very strong destructive power and extremely rapid velocity, which usually causes serious damage to infrastructure and residential areas downstream of the disaster (Xu et al. 2009; Zhang et al. 2015; Xing et al. 2015; Bi et al. 2016a; Li et al. 2016).

Countermeasures have been made to minimize the Geo-disaster's risk to downstream residential areas or transportation routes (e.g. protection gallery, flexible net, defending wall). Hauksson et al. (2007) conducted a series of laboratory experiments with granular material in order to reveal some kinetic relationships between snow avalanches and single mast-like obstacle. De Miranda et al. (2015) has proved that semi-rigid protection barriers are efficient to defend the rockfall hazard in Alps areas. Calvetti et al. (2016) have studied the interaction of mechanisms between the debris and rigid barriers. Bi et al. (2016b) conducted a series of numerical experiments to reveal the regulations between the rock avalanches' impact force and single defending structure. Nevertheless, protection gallery is suitable for the mountain traffic lines (Bi et al. 2016a), flexible net is mainly applied to debris flow protection (Song et al.2018a), while defending wall approach is not suitable for the steep terrain in the mountains for its high cost (Bi et al. 2016b).

Comparing to other protection methods, the arrays of baffle approach has its unique edge in terms of its low construction cost and strong constructability in complex areas (Song et al. 2017), such as steep natural terrain, etc. The traditional baffles system is composed of a number of ground-standing piles, which are usually installed downstream of the hazard source area and upstream of the target protection zone (Choi et al. 2014; Law et al. 2015). Relevant tests have revealed that baffle system can slow down and change the flow regime of debris flow (Ng et al. 2015). Current researches on baffles structure mainly focus on its protective mechanism. Ng et al. (2014) studied the interaction between granular flow and baffle structure through laboratory experiments and explored the influence of baffles arrangement on the flow regime of debris flow. Choi et al. (2014) studied the effects of baffles arrangement on the flow velocity of debris flow through numerical simulation. However, the studies conducted by the predecessors are limited due to their small-scale experiments and the weakness of the test results in terms of representation and promotion. Most researchers have only focused on the influence of some extrinsic factors such as baffle arrangement rather than how to improving its performance of energy dissipation. Some researchers have studied energy dissipation of geo-disasters; however, they only considered the kinetic properties such as the front velocities and neglected structures that are meaningful in practical engineering. Moreover, the selected research target is debris flow, which is quite different from rock avalanches in natural materials and composition as well as flow regimes.

In recent years, the baffles structure has also been proved as an effective way to prevent the rock avalanches by attenuating the kinetic energy (Bi et al. 2018a; Bi et al. 2018b): it is found that capacity of energy dissipation of baffles increases with increasing baffle row numbers and baffle row spacing, while it decreases with increasing baffle column spacing. Furthermore, increasing the array to four rows leads to nearly 50% reduction in maximum impact force. However, it is generally accepted by predecessors that the energy dissipation mechanism of the baffles system is mainly contributed by its arrangement (Choi et al. 2014; Ng et al. 2015; Bi et al. 2018b). In engineering practice, there are no more effective optimization measures other than changing the baffle spacing in energy dissipation; therefore, it is imperative to look for ways to enhance protection

abilities of the traditional baffles system.

Deceleration strip is another kind of energy dissipation system that consists of plenty of single nails (Figure 1) (Hou et al. 2010), which is commonly used in traffic engineering to limit the speed of vehicles around the sensitive sections such as school, hospital, and residential area (Meng and Zhang 2006). In the actual traffic engineering, pavement nails or pebbles are generally laid on sensitive sections, and continuous deceleration strip is carried out at intervals. Figure 1 (a) shows a schematic view of a vehicle passing through a deceleration strip. Deceleration strip can cause vehicles' vibration in some extent, which enhances the vehicle's kinetic energy dissipation. Figure 1 (b) shows the schematic diagram of the working condition to be set in this study: deceleration facilities are laid between the two arrays of baffles. The energy dissipation will occur when rock avalanche passes through the gap between baffles. Then the secondary energy consumption will be formed, when rock avalanche through the deceleration strip. With the deceleration strip installed, the kinetic energy of rock avalanches can be reduced continuously, so as to optimize the energy dissipation system of traditional array of baffles.

In this paper, the parameters that affect the joint energy dissipation efficiency of "baffles-deceleration strip" were analyzed. The three-dimensional discrete element method was used for numerical experiment, the parameters were chosen based on parameters inversion. Some crucial factors such as the nail number and the nail angle on impact force and flow velocity of rock avalanches were emphatically discussed. With specific studies above, some valuable conclusions will be drawn, which aim to provide a theoretical reference for the actual engineering application.

1 Numerical Model and Parameters

In order to obtain the parameters, parameter inversion should be carried out. The comparison between the indoor and numerical tests results are made in this section. A good agreement between these two results will demonstrate the validity of parameters selected. This is an important way to obtain parameters in discrete element simulation, which decides the reliability level of subsequent researches.

1.1 Rolling Resistance Linear Model

PFC3D software (Cundall & Strack 1979) was used in this study, and the mathematical model selected was the "Rolling Resistance Linear Model". The Rolling Resistance Linear Model is a new model in PFC3D that better reflects the actual movement of the block compared to the previous Linear Model. It is applied to model the contact behavior of solid particles and based on the linear model, to which a rolling resistance mechanism is added. It can be installed at both ball-ball and ball-facet contacts and implemented by picking the model in PFC3D. It is based on the linear model with the adding of rolling resistance mechanism, which makes its numerical results more consistent with the actual engineering investigation.

The importance of "Rolling Resistance Linear Model" in the practical engineering has been proved by many scholars (Iwashita & Oda 2002; Chen et al. 2016). In real granular systems, this mechanism may have different micro-mechanical origins, such as adhesion of the contact area, or the steric effect due to surface roughness or non-sphericity about the contact
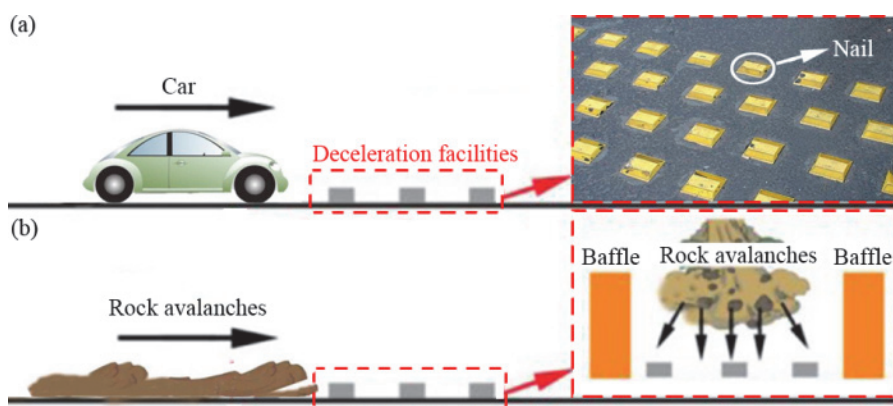

Figure 1 Schematic diagram of energy consumption in deceleration strip: (a) deceleration strip in traffic engineering, (b) deceleration strip to be used in this paper

point. The rolling resistance contact model provided in PFC3D is a simple model, based on the linear model, that incorporates a torque acting on the contacting pieces to counteract rolling motion.

The force-displacement law of the "Rolling Resistance Linear model" is expressed in the following form(Itasca 2016):

$$F_c = F^l + F^d, \quad M_c = M^T \tag{1}$$

where F^l is the linear force; F^d, the damping force; M^T, the rolling resistance moment. The linear and damping forces are consistent with the related parameters in the linear model. The rolling resistance moment is incremented as:

$$M^T := M^T - k_r \Delta \theta_b \tag{2}$$

where $\Delta \theta_b$ is the relative bend-rotation increment; the rolling resistance stiffness k_r can be defined as:

$$k_r = k_s \overline{R}^2 \tag{3}$$

where the $\overline{R}$ is the contact effective radius and can be defined as:

$$\frac{1}{\overline{R}} = \frac{1}{R^{(1)}} + \frac{1}{R^{(2)}} \tag{4}$$

As shown in Appendix 1, the $R^{(1)}$ and $R^{(2)}$ are the radii of end (1) and end (2) of the contact respectively. The $R^{(2)}$ will equal to ∞ in the situation of ball-facet contacts.

Two ways of energy dissipation are provided in the Rolling Resistance Linear Model. On one hand, E_{k_r} is the energy dissipated by the rolling strain in the linear spring. On the other hand, E_{μ_r} demonstrates energy dissipated by rolling friction. Appendix 2 demonstrates the energy

Figure 2 Flume model used to investigate rock avalanches interacting with a single baffle

dissipation of all rolling resistance linear models.

The rolling strain energy and rolling sliding energy can be calculated by

$$E_{\mu r} = \frac{1}{2} \frac{\|M^T\|^2}{k_r} \tag{5}$$

$$E_{kr} = E_{\mu r} - \frac{1}{2}((M^T)_o) + M^T) \cdot \Delta\theta_b^{\mu r} \tag{6}$$

where $\Delta\theta_b^{\mu r}$ is defined by

$$\Delta\theta_b^{\mu r} = \Delta\theta_b - \Delta\theta_b^k = \Delta\theta_b - (\frac{M^T - (M^T)_o}{k_r}) \tag{7}$$

where $(M^T)_o$ is the rolling resistance moment at the beginning of time.

1.2 Parameter inversion

1.2.1 Experimental device

The experimental equipment and measurement devices are already presented specifically in previous works (Wang et al. 2018), which are shown in Figure 2. Chute 1 is 8m long with a width of 0.35m, and the inclination is 46°. Chute 2 is 4m long with a width of 0.35m, and the inclination is 10.5°. The distance between the outlet of chute1 and the structure is n. A storage container is located at the top of channel, with a volume of 3 m3. Dry quartz particles with a diameter of 6 mm are contained in the storage container, and its outflow is controlled by a spring door. Nine stress sensors are set in the structure in this experiment. The measurement range of force sensor is 0~300 kPa (±0.05 kPa). Each area is $\pi \times 0.03^2$ m^2 and the total area is 0.0254 m^2. The impact forces were captured by sensors, which can be used for parameters inversion when comparing with the numerical results in the following steps.

The experimental procedure steps are summarized as follows: (1) Before measuring the impact pressure signal, pressure sensors, data acquisition system, SLR camera, and DV were mounted and calibrated. (2) A sieve analysis was then used to obtain the grain size distribution. The quantity of the solid particles was calculated and weighted. (3) The particles were hoisted to reservoir. (4) The particles were released through spring door. (5) The impact pressure was recorded using pressure sensors and a data acquisition system. Meanwhile, the flowing regime was recorded by cameras. (6) The platform was cleaned. (7) The solid particles were reset and the above steps were repeated.
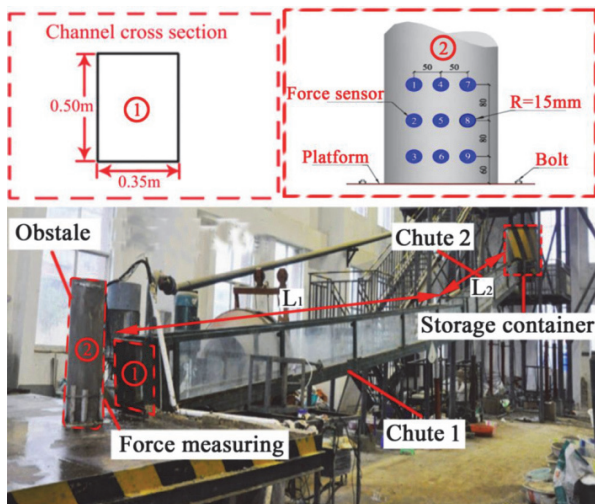
1.2.2 Comparison of results

The properties of particles, for example the size, shape, and input material parameters, play a leading role in discrete element (DEM) simulation. What is more, the most difficult part is input material parameters calibration. Although the DEM allows the fundamental particle motions of bouncing, falling, sliding, and rolling to be modeled, some input parameters pertaining to these motions are difficult to determine and quantify accurately and reliably to ensure that input parameters and modeling techniques are appropriate for simulating the interaction of flow against avalanche baffles. At present, there are a lot of methods to obtain the input parameters (Zhao & Shan 2013; Shan & Zhao 2014; Zhao 2014). In this paper, there are two major similitudes to determine the parameters in DEM simulation, especially the avalanche-structure interaction: deposition similarity and impact similarity. Deposition similarity is achieved by the comparison of the deposition shape between the physical experiment and the DEM simulation at different time steps. Impact similarity refers to the comparison of the impact force between or among experiments.

The comparison of the results of experiments and simulation at different time steps is shown in Appendix 3. At t=1.20s, the particles are accumulated around the bearing structure, whereas the deposition area is small, looking like an approximately isosceles triangle. From t=1.20 to t=4.15, the triangle gradually disappears, the particles around the structure increase as time goes on. From t=6.42s, a "butterfly shape" with a left and right symmetry has been formed. When t=9.12s the accumulation area continues to increase and the "butterfly shape" becomes more obvious.

In addition to the resemblance of deposition morphology, the previous study (Bi et al. 2018b) also covered the variation of the maximum impact force with the distance of the structure. As indicated in Appendix 4, the measured data in each point is higher than the calculated data, but both data meet similar laws: the maximum impact force decreases with the increasing distance between the obstacle and chute terminal. Those of the simulation are higher than those of the laboratory due to the fact that many gaps exist between the force conductive sensors to capture all the impact forces. However, both the experiments share a similar force changing trend.

The material parameters used in this numerical simulation were gained after matching the results of the numerical experiment with the laboratory test. Appendix 5 summarizes the material parameters obtained by this parameter inversion, which were used for a series of further research in this paper.

2 Model description and Parameters

Based on the above parameters, a numerical model of "baffles-deceleration strip" was established in this paper. And then a numerical model was built using PFC3D to carry out a series of analysis.

2.1 Project background

The Wenchuan earthquake on May 12, 2008, triggered numerous landslides within the seismic fault zone. The Wangjiaya landslide occurred within the major seismic faults, as shown in Figure 3(a) (Yin et al. 2015). In totality, the geological environment of this area is very fragile in terms of cliffy terrain, high annual rainfall, weak rock and fractured rock stratum.

As shown in Figure 3(a), the engineering point selected in this study is located between Beichuan and Maoxian (104°17'16" E, 31°41'33" N), 21.3 km on the southwestern side of Beichuan (cross mark in Figure 3(a)). The height between the souce area and slope toe is 64.5 m. The upper terrain is steep (50°), whereas the lower terrain gently slopes at an angle of about 20°. Preliminary estimate of the potential detached rock volume is 0.18×10^5 m³ according to measurements, which is located at a disaster-prone area with a high probability of secondary disasters on account of severe rainfall. Figure 3(b) demonstrates the scene diagram of specific working condition in this study, in which the flow direction of rock avalanche, the placement area of the protective structure and the location of residential areas to be protected are demonstrated. As seen from Figure 3(b), when the rock avalanches pass through the baffles system, the energy will be attenuated, resulting in the decline of its kinetic energy, and thus reducing the impact
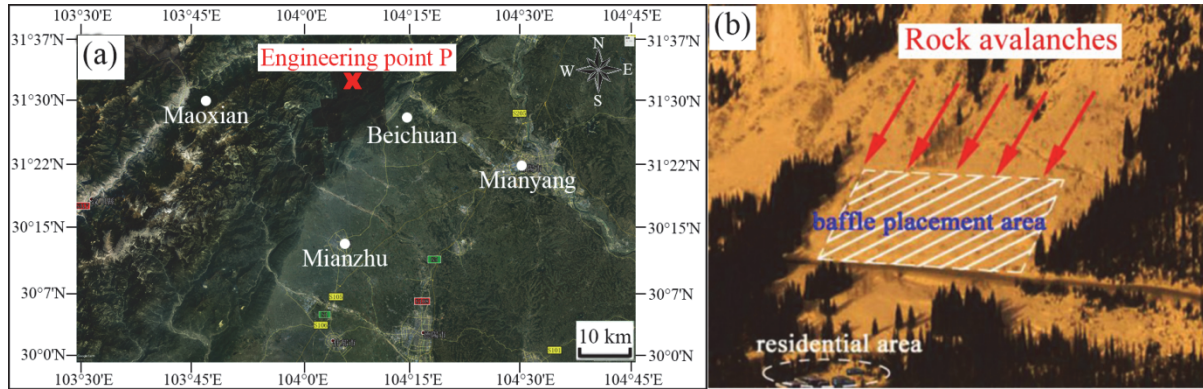
Figure 3 Study site and the distribution of disasters in the surrounding area: (a) location of specific project, (b) Scene diagram of specific engineering case in this study

of rock avalanches on the structure.

2.2 Numerical modeling

The physical model of the working conditions is shown in Figure 4, which simplifies the actual conditions and can be used to study the relationship between rock avalanches, protection structure, and bearing structure. The particle material selected in this numerical is in agreement with above parameters in the inversion. Based on in situ observation of the landslide area, the adopted particle diameter ranged from 0.1m to 1.0 m, which generated randomly in PFC3D. Although the shape of particles plays an important role in the granular flow movement, the influence trend of impact force exerted by them is consistent (Gao & Meguid 2018). Moreover, it has been proved that choosing spherical particles is feasible for rock avalanche studies (Bi et al. 2016b). In addition, the wall element parameters are also consistent with the above parameter inversion.

As shown in the Figure 5, a schematic diagram of the simplified 3-D physical model is established according to actual engineering which is mentioned above. The slope is divided into three parts. The length of the upper part, middle part, and lower part is L1, L2, L3, respectively. The angle of the upper part of the slope is α, the middle is β, and the lower is 0. The figure shows the specific location of the source and baffles. h, l, and w represent the height, length and width of a single baffle, respectively. n_c and n_r denotes the length of the clearance of the baffles in the direction of X and Y. Four different working conditions of the deceleration strip have been set up in this study. In which case 1 only contains the array of baffles, case

2 adds a deceleration strip in the X direction interval of each row of array of baffles, while case 3 adds two, and case 4 adds three. The specific distribution is shown in the diagram, in which the length, width and height of the deceleration nail are all 1m. The angle of the nail body is γ. Table 1 lists the specific parameters of these working conditions.

The illustration of "avalanches - baffle - deceleration strip - structure" in the practical project is shown in Figure 5. The destruction extent of rock avalanches to the structure usually depends
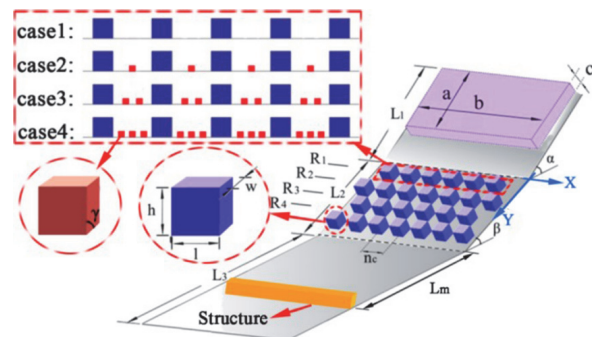

Figure 4 Physical model of the working conditions.

Table 1 Geometrical parameters of slope and defending baffles

Description	Symbol	Value
Avalanche length (m)	a	36.0
Avalanche width (m)	b	84.0
Avalanche depth (m)	c	6.0
Slope angle 1 (°)	α	50.0
Slope angle 2 (°)	β	20.0
Slope length 1 (m)	L1	60.0
Slope length 2 (m)	L2	54.0
Slope length 3 (m)	L3	200.0
Horizontal baffle length (m)	l=w	6.0
Vertical baffle length (m)	h	6.0
Baffle spacing in x direction (m)	n_c	12
Baffle spacing in y direction (m)	n_r	6

on the energy dissipation of the protection system. The structure was set up at the bottom of slope in this study in order to record and study the impact force of rock avalanches through the different energy dissipating system. The destructive index of rock avalanches to the structure was represented by the maximum impact force. The energy dissipation efficiency of each working condition was judged by comparing the maximum impact force of rock avalanches to the structure under different working conditions. As shown in Figure 5, the size of the bearing structure was large enough to block all rock avalanches without any kinetic energy losing. As seen in Figure 5, the rock avalanches material in simplification case may not have the same impact energy compared with the actual case due to the different shape of source area. However, this paper aimed to study the regular variation of impact energy for qualitative analysis rather than quantitative examination. Model simplification would make the analysis simpler and easier.
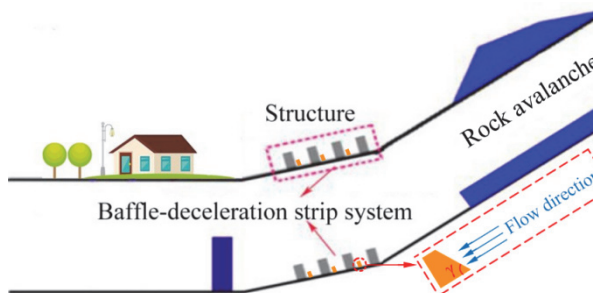

Figure 5 Illustration of "Avalanches-baffle-deceleration facility-structure" model: (a) Model of practical engineering.(b) Simplified model.

In PFC3D, the slope, baffles and deceleration strip are all constructed by wall unit, and the bearing body (debris flow) is made up of a ball unit. The energy dissipation of the structure is only considered under the effect of gravity. Spherical units from 0.1 meter to 1 meter are generated randomly. And the different sizes of particles in actual working condition are fully considered in

this simulation. The parameters in this study are same as that of the previous parameter in Appendix 5, whereas the parameters of the specific working conditions are shown in Table 2. The change of nail angle and nail numbers are considered as the parameters to investigate the mechanism of system's energy dissipation. Figure 5 shows that the angle of nail in the flow direction side changes. The smaller the angle γ, the smaller the volume of nail. Thus, more material can be saved in practical engineering.

3   Results Analysis

The following studies were performed using the software PFC3D, a simulation tool based on the distinct element method for modeling the dynamic motion and interaction of assemblies of arbitrarily sized spherical particles. This study mainly focuses on how the deceleration strips optimize the traditional baffles protection system. The influence of the number and angle of a single nail was analyzed. In addition, the effect of the new protection system on structures at different distance was considered.

3.1 Influence of nails number on impact force

The effect on the maximum impact force caused by the distance of L_m when the angle of the single nail is γ is shown in Figure 6. The changing trends of different nail angles with different nail numbers are similar in Figure 6. Furthermore, the influence of nails number on impact force is the main topic in this section, thus, a typical example of γ=30° is discussed here. When the distance between the structure and the foot of the slope is 30m in Figure 6(a), the maximum impact force under case 1, case 2, case 3, and case 4 are, $3.75×10^7$ N, $3.49×10^7$ N, $3.31×10^7$ N, $3.05×10^7$ N, respectively. Generally, the maximum impact force

Table 2 Condition setting of various working conditions

Case number	Nail Numbers	Schematic diagram	Nail Angle (γ)	The distance from the structure to the slope toe(m)
1	None		None	30, 40, 50, 60, 70, 80, 90
2	1 interval		30°, 45°, 60°, 90°	30, 40, 50, 60, 70, 80, 90
3	2 intervals		30°, 45°, 60°, 90°	30, 40, 50, 60, 70, 80, 90
4	3 intervals		30°, 45°, 60°, 90°	30, 40, 50, 60, 70, 80, 90
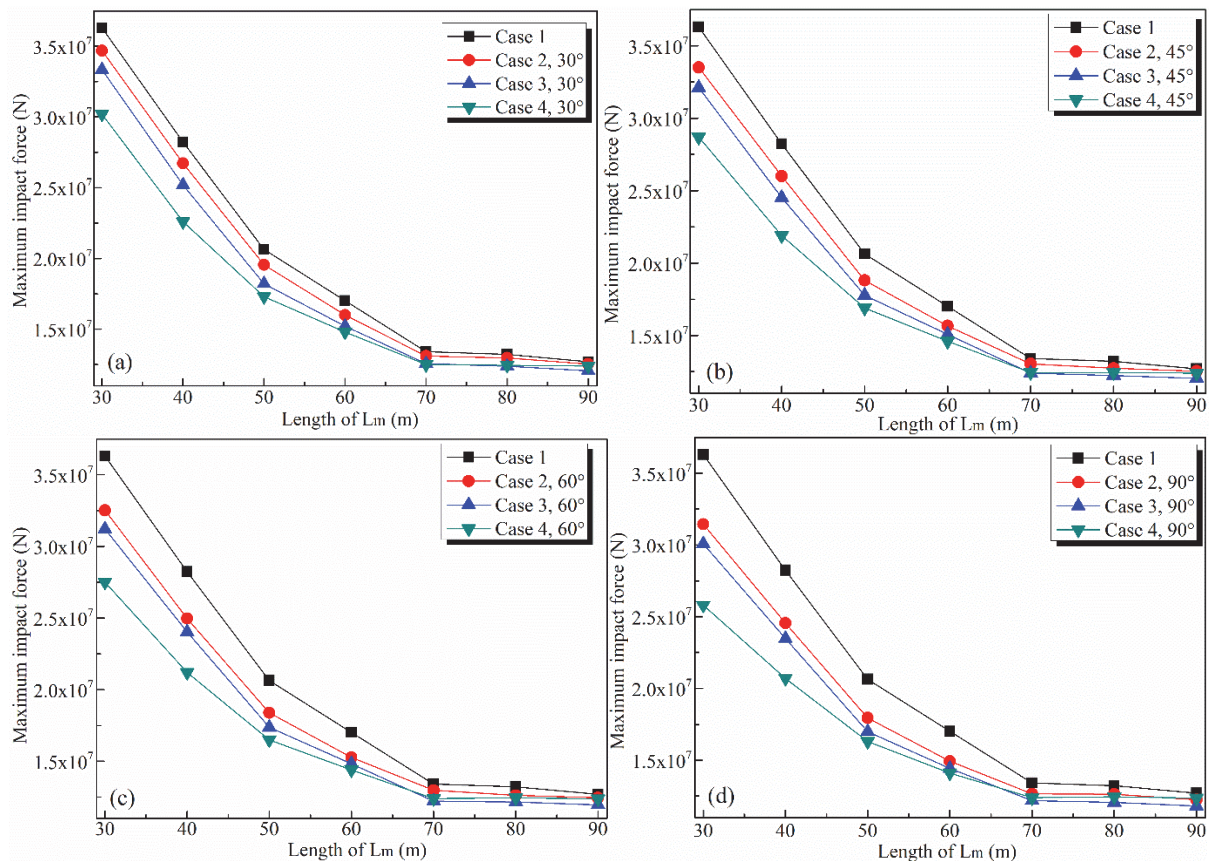
Figure 6 The impact of different conditions on the maximum impact: (a) γ=30°; (b) γ=45°; (C) γ=60°; (D) γ=90°

of each condition decreases with the increase of the length of L_m. There is a rule to follow: the maximum impact force of case 1 > the maximum impact force of case 2> the maximum impact force of case 3> the maximum impact force of case 4. Hence, increase the distance of bearing structure can effectively reduce the maximum impact force of rock avalanches. Even for Case 1, the maximum impact force is almost similar to the other Cases at L_m=70 to 90m. This is because the long length of L_m (L_m=70 to 90m) enables the particles case more energy dissipation through particle collision and particle friction. Thus, when $L_m > 70m$, the subjective factor that lead to the disaster energy dissipation is the length of L_m; when $L_m < 70m$, the subjective factor that lead to the disaster energy dissipation is the nail numbers.

The changing trend about other nail angles with different nail numbers are similar to the case of γ=30° in Figure 6(a). The typical example of γ=30° is discussed here. Figure 7 demonstrates the relationship between nail numbers and maximum im pact force under the conditions of different

length of L_m. When the L_m is short (30m), increasing the nail numbers can effectively reduce the maximum impact force: The maximum impact force of the case 4 is reduced by 0.5×10^7 N when compared with the case 1. When the length of L_m increases to 60m, the maximum impact force of the case 4 is only reduced by 0.2×10^7 N. The ability to reduce the maximum impact force which caused by
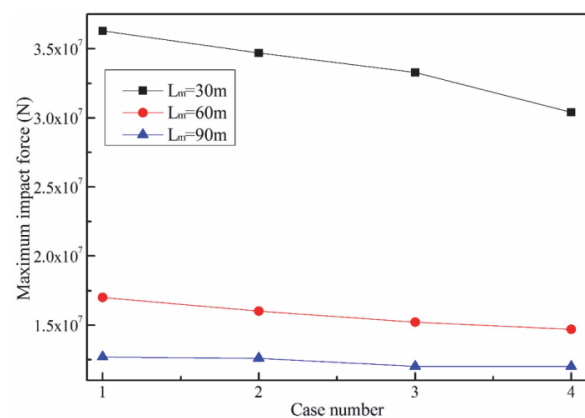

Figure 7 The relationship between the number of retarders and the maximum impact force.

increasing the nail numbers is no longer obviously. When the length of L_m increases to 90m, increasing the nail numbers has almost no effect on the variation of the maximum impact force.

In order to explain this phenomenon, structures in case 1, case 2, and case 3 with inclination of γ = 90° were selected in this study. And then, the velocity variation of rock avalanches crossing through the protection system under different time steps was analyzed. It can be seen from Figure 8 that when t = 6.52s, the tail of rock avalanches in case 1 is kept horizontal alignment with the row R1 (in figure 5), while the tails of rock avalanches in case 2 and case 3 are stayed above the row R1. When t = 9.50s, the tail of the rock avalanches in case 1 is located between the row R3 and row R4, while the tail of the rock avalanches in case 2 is stayed between the row R2 and row R3, and the tail of the rock avalanches in case 3 is located between the row R1 and row R2.When t = 12.20s, a similar rule can still be obtained: movement distance of tail in case 1 > movement distance of tail in case 2 > movement distance of tail in case 3. To conclude, it will cause more energy dissipation for rock avalanches crossing through hybrid system as the nails number increases. Hence, increasing nails number makes the impact force reducing.

3.2 Effects of different nail angle on impact force

Figure 9 shows when nail angle changes, how the maximum impact force varies with the change of the length of L_m. Figure 9 (a) shows the case 2, Figure 9 (b) shows the case 3 and Figure 9 (c) shows the case 4. When the length of L_m is the smallest (30m), the impact force acting on the structure body is the largest. As the length of L_m increases, the impact force gradually decreases. When the length of L_m is 70m or more, the maximum impact force remains almost unchanged. The same rule is also shown in Figure 9 (b) and Figure 9 (c). Moreover, Figure 9 shows that as the nail angle γ increases, the maximum impact force of the rock avalanches decreases.

The changing trend about other cases with different nail angles are similar to the case 2 in Figure 9, furthermore, the influence of nails angle on impact force is the main topic in this section,
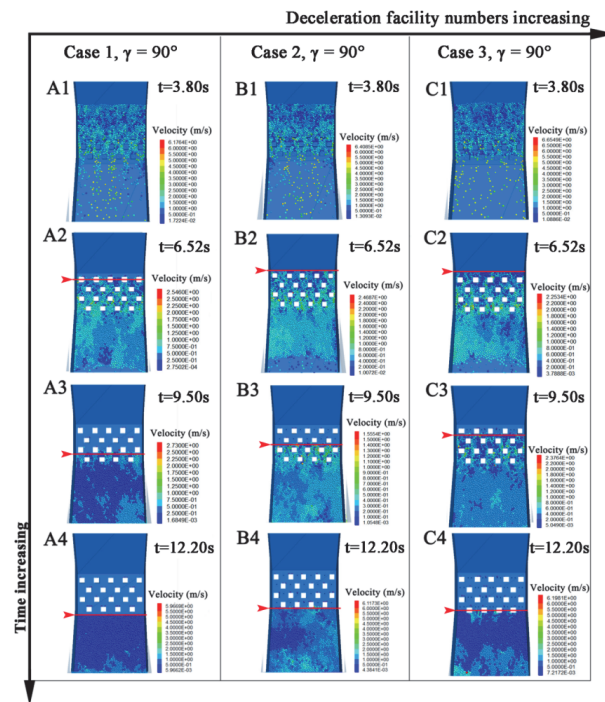

Figure 8 Effect of number of retarders on kinetic energy of debris flow

thus, a typical example case 2 is discussed here. Figure 10 shows when the length of L_m changes, how the maximum impact force varies with the change of nail angle. As can be seen from the figure, when the length of L_m is 30m, the effect of the angle γ of the nail on the maximum impact force is obvious. When γ increased from 30 ° to 60 °, the maximum impact force decreased from 3.45×10^7 N to 3.21×10^7 N. When γ increased from 60 ° to 90 °, the maximum impact force decreased from 3.21×10^7 N to 3.15×10^7 N. When the length of L_m is 60m, the effect of the angle γ of the dissipater on the maximum impact force is weakened, and the slope of the maximum impact force caused by different angle of the nail also reduces. When the length of L_m is 90m, the effect of the angle γ on the maximum impact force can be almost neglected.

Similarly, in order to explain the phenomenon above, this study analyzed the effect of the nail with different angle γ on the kinetic energy of rock avalanches in case 3 to illustrate the problem (Figure 11). When t = 6.52s, the movement distance of tail flow for γ= 30 ° is slightly larger than those of γ= 45 ° and γ= 60 °. Whereas, when γ= 45 ° and γ= 60 °, the movement distance of debris tail is almost the same. When t = 9.50s and t = 12.20s, the movement distance of the three started to show
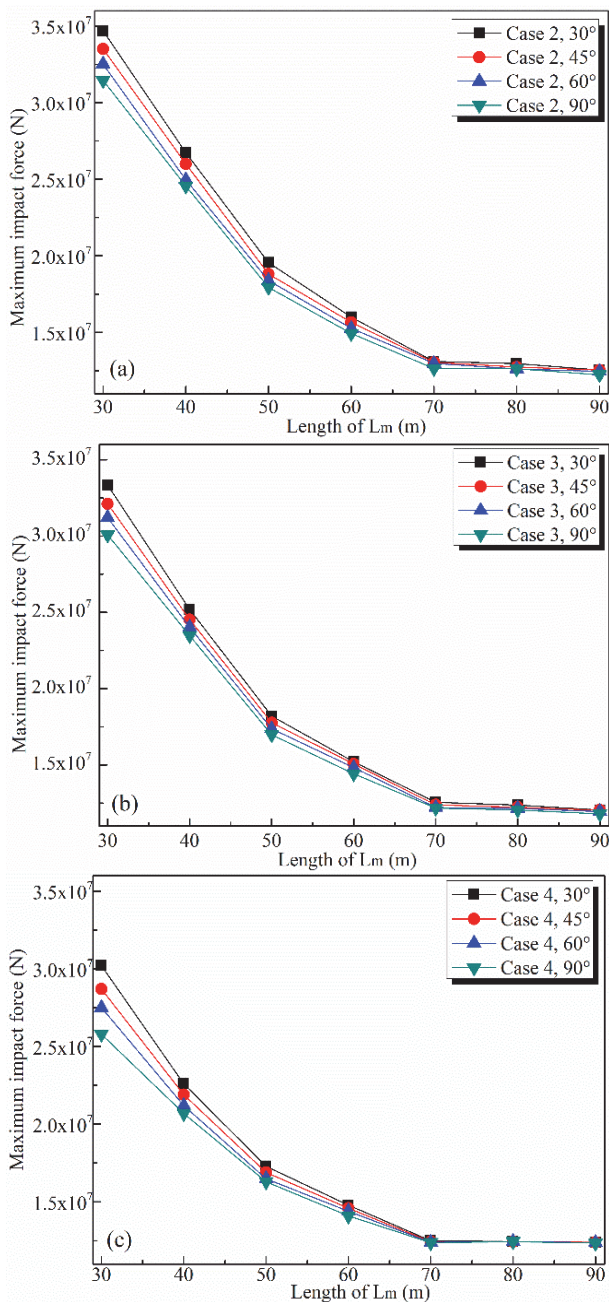
Figure 9 Trends of maximum impact force with structure distance under different γ values: (a) Case 2; (b) Case 3; (C) Case 4

observation points were set in the gaps of each row of energy dissipating systems. The velocities of all the particles passing through were recorded, and the average values were obtained. Finally, the average velocity of debris flows across each row of energy dissipating system was obtained. In this study, we make reference to the analyze method of granular flow kinetics which proposed by Savage and Hutter (1989). The non-dimensional movement time $t*$ and the flow velocity $U*$ can be respectively defined in the progressive process of general particle flow along the slope. With these
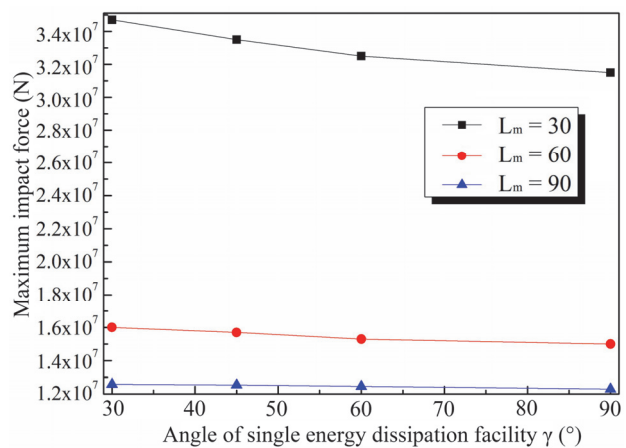

Figure 10 Variation of maximum impact with γ at different structure distances

a clear difference: movement distance of dragon tail when γ= 30 °>movement distance of dragon tail when γ= 45 °>movement distance of dragon tail when γ= 60 °. It can also be seen that increasing the angle of the nail can effectively reduce the kinetic energy of the rock avalanches so as to reduce its maximum impact on the structure.

Figure 12 shows the average velocity over time of a rock avalanches going through each row of energy dissipating systems. In this study,
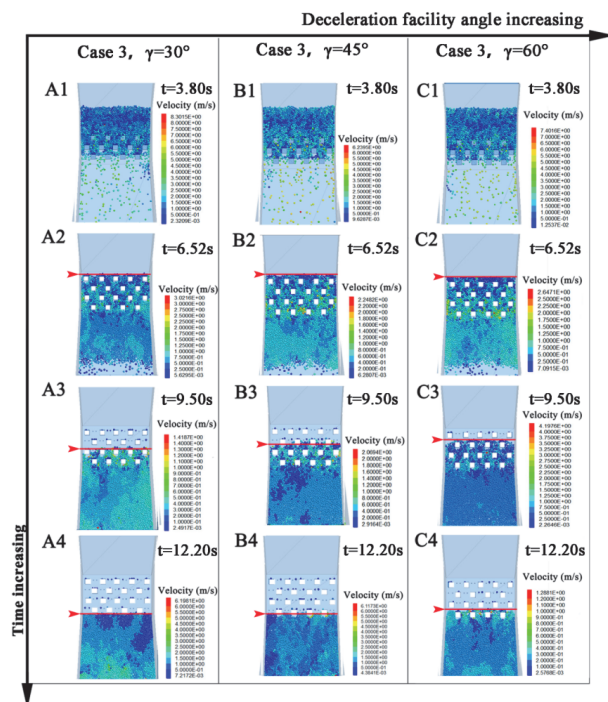

Figure 11 Effect of nail angleγon the kinetic energy of debris flow

parameters the initial size effect of the particle stack prior to its start-up can be considered so that the particle flow at different scales is comparable:

$$t^* = t/\sqrt{L_0/g} \qquad (8)$$

$$U^* = U/\sqrt{gL_0} \qquad (9)$$

where t is the flow time, L_0 is the initial particle length, g is the acceleration of gravity, U is the flow velocity.

Figure 12 (a) shows the velocity versus time for the rock avalanches to pass through the energy dissipating system R1. It can be seen from the figure that when the rock avalanches pass through the energy dissipating system with only baffles (case 1), the speed values at each time point are greater than or equal to that of the other two conditions. Figure 12 (b) shows that the energy dissipating system in case 3 and with γ= 60 ° has good energy dissipation characteristics when passing through the second row of energy dissipating systems. The rock avalanches velocity through this row is clearly less than that of the other two working conditions. Figure 12 (c) shows that the energy dissipation efficiency on the three operating conditions is significantly different when the rock avalanches passes through the third row of energy dissipating systems. Among them, the rock avalanches velocity is the highest in case 1; the rock avalanches velocity in case 3 with γ= 30 ° is the second; the rock avalanches velocity in case 3 with γ= 30 ° is the slowest. Figure 12 (d) shows that the variation of rock avalanches velocities in case 3 with γ= 30 ° and γ= 60 ° is almost the same when passing through the fourth row of energy dissipating systems. Whereas the rock avalanches rate in case 1 before $t^*= 6$ is far greater than in the other two cases. However, the rate in these three cases gradually approaches to each other after $t^*= 6$.
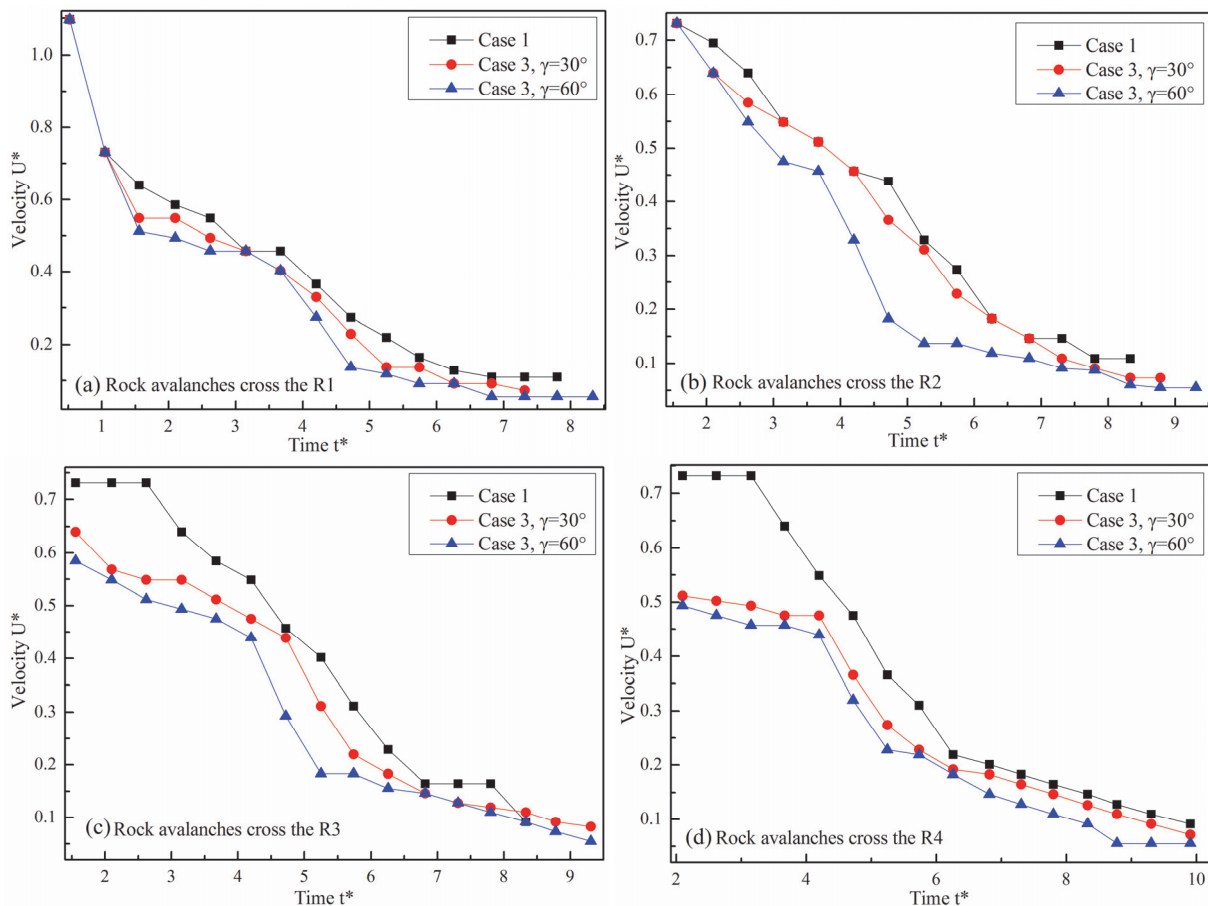

Figure 12 Velocity variation of debris flows across energy dissipating systems: (a)The velocity variation of debris flows through the dissipating system R1; (b)The velocity variation of debris flows through the dissipating system R2; (c)The velocity variation of debris flows through the dissipating system R3; (d)The velocity variation of debris flows through the dissipating system R4.

3.3 Energy dissipation mechanism

The selected observation area in PFC3D model, which is used for further researches about hybrid system's energy dissipation mechanism, is shown in Figure 13. Figure 14 shows that the process of particles crossing through the observation area at different time steps. The investigation about avalanches fragments movement when they passing through structures(baffles, nails) gaps is important to unveil the mechanism of energy dissipation. For this reason, it has focused much of its attention on the three gaps (A, B, and C) in Figure 14. It can be seen from Figure 14 that these three gaps have nearly no particles at t = 0.45 s. Particles begin accumulate in these three gaps from t = 2.25 s. From t = 4.05 s to t = 5.40 s, particles accumulation tend to stabilize. Fine particles are found obviously from t = 0.45 s to t = 2.70 s, however, from t = 3.15 s to t = 5.40 s, coarse particles are more obviously found in the Figure 15.

3.3.1 Blocking effects caused by segregation process

Figure 15 shows that a cross section about Figure 14 (C_1-C_2) has been selected for further observation. Figure 15 shows obviously that segregation has been generated during the process of particles movement: the coarse particles are floated in the fine particles. The current design of defending structures does not explicitly consider the effects of segregation in rock avalanches. However, some scholars (Song et al. 2018b) have proved that segregation is crucial for geo-hazards impact force and its flow regime. Segregation effect exists in the rock avalanches movement process (Bi et al. 2016b).

The segregation results in the coarse particles float on the top and the small sink to the bottom during the movement process (Figure 16 (a)). On the condition of the same material density, large particles of the same velocity tend to have higher kinetic energy, making them easier to jump over the nail. Fine particles are blocked by nails (Figure 16 (b)), hence causing the energy dissipation. Increasing the angle γ of the nail increases the ability of large particles jumping. In addition,

increasing the number of nails makes the particle bridge easier to form. Both methods can effectively reduce the kinetic energy of rock avalanches.
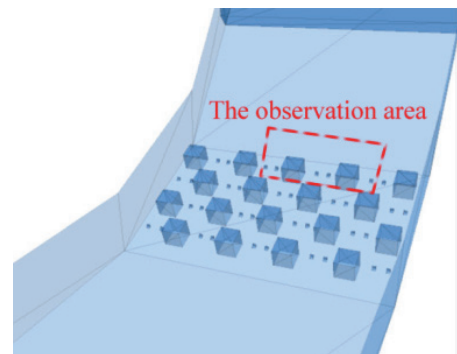

Figure 13 Observation area in PFC3D model

3.3.2 Effects of Particles Bridge

Figure 14 shows that particles hold together and move as one before they reach the R1 of baffle system. When particles reach the R1, side particles will be stopped by the blocking effect of baffles. Whereas particles in the middle part have four main ways for particles passing through the gaps between two baffles (Figure 17(a)): (I) coarse particles and fine particles are all pass through the gaps between baffle and nail directly, (II) fine particles pass around the nail, (III) coarse particles pass over the nail, (IV) coarse particles pass over the fine particles bridge. All of these mechanisms can cause energy dissipation expect the (I).

Figure 17(b) shows that formation of a particles bridge between different structures (nails and baffles) during the granular flow movement.
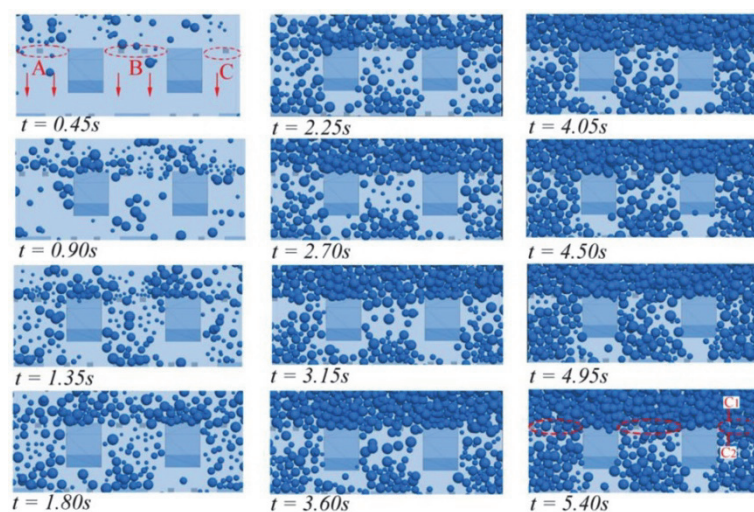

Figure 14 Particles crossing through the observation area at different time steps
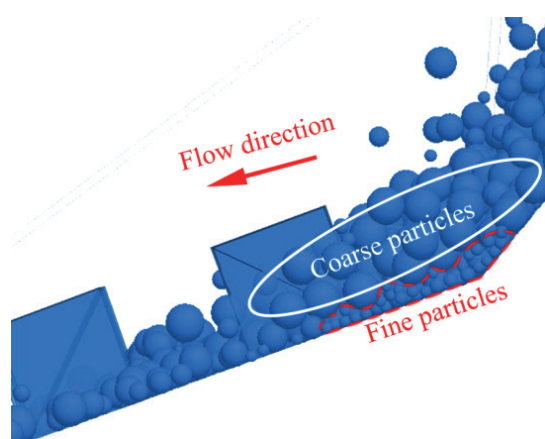
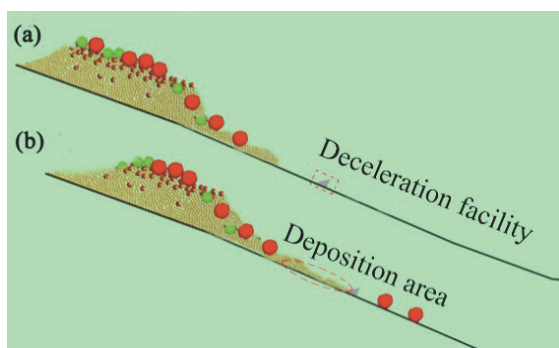**Figure 15** Cross section about Figure 15 (C1-C2)

Figure 16 Schematic diagram of the rock avalanchesthrough the nail in the role of sorting.
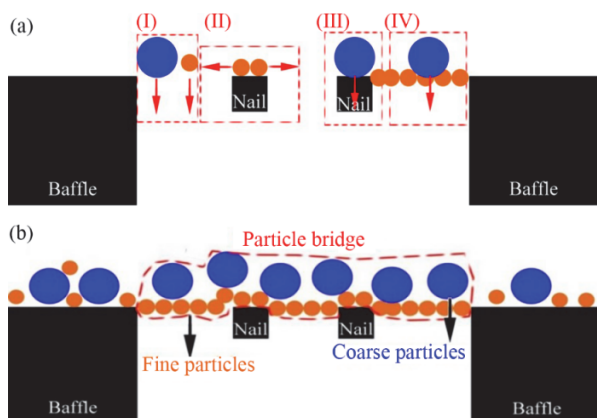

Figure 17 Schematic diagram (a) Methods for particles passing through the gaps; (b) Particles bridge between structures.

The particles bridge contains two layers for the reason of segregation: the upper layer is coarse particles, while the lower layer is fine particles. Coarse particles overflow from fine particles instead of crossing directly from gaps. As the fine particles layer is rougher than slope surface, more energy dissipation will be generated.

4   Conclusion

Effects of "baffles - deceleration strip" hybrid protection system are discussed specifically in this paper. With the deceleration strip installed, traditional baffles system was optimized. Some key factors (such as the nails angle, the nails number) were emphasized and studied for its dissipation efficiency by series of numerical experiments. Parameters selected were obtained through the parameters inversion by comparing laboratory and numerical experiments. This article gets the following conclusion through the numerical analysis:

(1) Increasing the nails number can improve the energy dissipation efficiency of the hybrid system. Moreover, it can also reduce the maximum impact force effectively. Increasing the nails angle also follows the above rules.

(2) Under the same baffle conditions, increasing the number of nails can increase the blocking ability for fine particles effectively, and increasing nails angle can enhance the blocking ability for the coarse particles effectively. This is because increasing the number of nails can makes Particles Bridge forming effectively. Moreover, increasing the nails angle leads to more energy dissipation for coarse particles.

(3) Furthermore, the influences of the nails number and nails angle on the maximum impact force are related to the value of L_m. When value is small, the influence is great: increasing the nails number or angle will make more variation of maximum impact force (L_m=30m). Whereas, the influence will decreases as the value increases (L_m=70m).

(4) There are mainly three ways for nails attenuate rock avalanches: (i) block the fine particles directly; (ii) form the particles bridge between nails and baffles; (iii) dissipate the coarse particles energy directly.

Hence, it is advisable to use baffles - deceleration strip hybrid system rather than traditional baffle system during the practical engineering design for its significant energy dissipation effects.

Acknowledgements

Electronic supplementary material: Supplementary material (Appendixes 1 to 5) is available in the online version of this article at https://doi.org/10.1007/s11629-018-4908-3.

References

Bi YZ, He SM, Li XP, et al. (2016a) Geo-engineered buffer capacity of two-layered absorbing system under the impact of rock avalanches based on Discrete Element Method. Journal of Mountain Science 13(5): 917-929.
https://doi.org/10.1007/s11629-014-3354-0

Bi YZ, He SM, Li XP, et al. (2016b) Effects of segregation in binary granular mixture avalanches down inclined chutes impinging on defending structures. Environmental Earth Sciences 75(3): 263-268. https://doi.org/10.1007/s12665-015-5076-1

Bi Y Z, He S M, Du Y J, et al. (2018a) Effects of the configuration of a baffle–avalanche wall system on rock avalanches in Tibet Zhangmu: discrete element analysis. Bulletin of Engineering Geology and the Environment: 1-16.
https://doi.org/10.1007/s10064-018-1284-8

Bi YZ, Du YJ, He SM, et al. (2018b) Numerical analysis of effect of baffle configuration on impact force exerted from rock avalanches. Landslides 15(5): 1029-1043.
https://doi.org/10.1007/s10346-018-0979-z

Choi CE, Ng CWW, Song D, et al. (2014) Flume investigation of landslide debris–resisting baffles. Canadian Geotechnical Journal 51(5): 540-553. https://doi.org/10.1139/cgj-2013-0115

Cundall PA, Strack ODL. (1979) A discrete numerical model for granular assemblies. Geotechnique, 29(1): 47-65.
https://doi.org/10.1680/geot.1979.29.1.47

Gao Ge, Meguid M A. (2018) On the role of sphericity of falling rock clusters—insights from experimental and numerical investigations. Landslides 15(2): 219-232.
https://doi.org/10.1007/s10346-017-0874-z

Hou S, Sun X, He Y, et al. (2010) Vehicle's Shock Absorbing Capacity and Roadway Rumble Strips[M]//ICCTP 2010: Integrated Transportation Systems: Green, Intelligent, Reliable: 585-590. https://doi.org/10.1061/41127(382)62

Hungr O, Leroueil S, Picarelli L. (2014) The Varnes classification of landslide types, an update. Landslides 11(2): 167-194.
https://doi.org/10.1007/s10346-013-0436-y

Itasca, Consulting Group Inc., (2016) PFC3D Particle Flow Code in 3 Dimensions. User's Guide. Minneapolis.

Iwashita K, Oda M. (2000) Micro-deformation mechanism of shear banding process based on modified distinct element method. Powder Technology 109(1): 192-205.
https://doi.org/10.1016/S0032-5910(99)00236-3

Law RPH, Choi CE, Ng CWW (2015) Discrete-element investigation of influence of granular rock avalanches baffles on rigid barrier impact. Canadian Geotechnical Journal 53(1): 179-185.
https://doi.org/10.1139/cgj-2014-0394

Li X, Wu Y, He S, et al. (2016) Application of the material point method to simulate the post-failure runout processes of the Wangjiayan landslide. Engineering Geology 212: 1-9.
https://doi.org/10.1016/j.enggeo.2016.07.014

Meng J P, Zhang J F. (2006) The effect of deceleration strips upon traffic flow. Modern Physics Letters B 20(14): 835-841.
https://doi.org/10.1142/S0217984906010950

Ng CWW, Choi CE, Kwan JSH, et al. (2014) Effects of baffle transverse blockage on landslide debris impedance. Procedia Earth and Planetary Science 9: 3-13.
https://doi.org/10.1016/j.proeps.2014.06.012

Ng CWW, Choi CE, Song D, et al. (2015) Physical modeling of baffles influence on landslide debris mobility. Landslides 12(1): 1-18.
https://doi.org/10.1007/s10346-014-0476-y

Chen Z, Omidvar M, Li K, et al. (2016) Particle rotation of granular materials in plane strain. International Journal of Physical Modelling in Geotechnics 17(1): 23-40.
https://doi.org/10.1680/jphmg.15.00046

Savage SB, Hutter K (1989) The motion of a finite mass of granular material down a rough incline. Journal of fluid mechanics 199: 177-215. https://doi.org/10.1017/S0022112089000340

Shan T, Zhao J. (2014) A coupled CFD-DEM analysis of granular flow impacting on a water reservoir. Acta Mechanica 225(8): 2449-2470. https://doi.org/10.1007/s00707-014-1119-z

Song D, Ng CWW, Choi CE, et al. (2017) Influence of debris flow solid fraction on rigid barrier impact. Canadian Geotechnical Journal 54(10): 1421-1434. https://doi.org/10.1139/cgj-2016-0502

Song D, Choi CE, Ng CWW, et al. (2018a) Geophysical flows impacting a flexible barrier: effects of solid-fluid interaction. Landslides 15(1): 99-110. https://doi.org/10.1007/s10346-017-0856-1

Song D, Choi CE, Zhou GGD, et al. (2018b) Impulse Load Characteristics of Bouldery Debris Flow Impact. Géotechnique Letters: 1-25. https://doi.org/10.1680/jgele.17.00159

Wang D, Chen Z, He S, et al. (2018) Measuring and estimating the impact pressure of debris flows on bridge piers based on large-scale laboratory experiments. Landslides 15(7): 1331-1345.
https://doi.org/10.1007/s10346-018-0944-x

Xing AG, Xu Q, Gan JJ (2015) On characteristics and dynamic analysis of the Niumian valley rock avalanche triggered by the 2008 Wenchuan earthquake, Sichuan, China. Environmental Earth Sciences 73(7): 3387-3401.
https://doi.org/10.1007/s12665-014-3626-6

Xu Q, Fan X M, Huang R Q, et al. (2009) Landslide dams triggered by the Wenchuan Earthquake, Sichuan Province, south west China. Bulletin of engineering geology and the environment 68(3): 373-386. https://doi.org/10.1007/s10064-009-0214-1

Yin Y, Li B, Wang W (2015) Dynamic analysis of the stabilized Wangjiayan landslide in the Wenchuan Ms 8.0 earthquake and aftershocks. Landslides 12 (3) 537–547.
https://doi.org/10.1007/s10346-014-0497-6

Zhang Y, Guo C, Lan H, et al. (2015) Reactivation mechanism of ancient giant landslides in the tectonically active zone: a case study in Southwest China. Environmental Earth Sciences 74(2): 1719-1729. https://doi.org/10.1007/s12665-015-4180-6

Zhao J, Shan T (2013) Coupled CFD–DEM simulation of fluid–particle interaction in geomechanics. Powder technology 239: 248-258. https://doi.org/10.1016/j.powtec.2013.02.003

Zhao T (2014) Investigation of Landslide-induced Debris Flows by the DEM and CFD. University of Oxford.

Zhou GGD, Ng CWW (2010) Dimensional analysis of natural debris flows. Canadian Geotechnical Journal 47(7): 719-729.
https://doi.org/10.1139/T09-134